Optimization of Micromachined Photon Devices

B.M. Evans III*[a], P.G. Datskos[a,b], S. Rajic[a], and I. Datskou[c]

[a]Oak Ridge National Laboratory, MS 8039, Oak Ridge, TN 37830
[b]University of Tennessee, Department of Physics, Knoxville, TN, 37996-1200
'Environmental Engineering Group, 11020 Solway School Rd., Knoxville, TN 3793 I

ABSTRACT

The Oak Ridge National Laboratory has been instrumental in developing ultraprecision technologies for the fabrication of optical devices. We are currently extending our ultraprecision capabilities to the design, fabrication, and testing of micro-optics and MEMS devices. Techniques have been developed in our lab for fabricating micro-devices using single point diamond turning and ion milling. The devices we fabricated can be used in micro-scale interferometry, micro-positioners, micro-mirrors, and chemical sensors. In this paper, we focus on the optimization of microstructure performance using finite element analysis and the experimental validation of those results. We also discuss the fabrication of such structures and the optical testing of the devices. The performance is simulated using finite element analysis to optimize geometric and material parameters. The parameters we studied include bimaterial coating thickness effects; device length, width, and thickness effects, as well as changes in the geometry itself. This optimization results in increased sensitivity of these structures to absorbed incoming energy, which is important for photon detection or micro-mirror actuation. We have investigated and tested multiple geometries. The devices were fabricated using focused ion beam milling, and their response was measured using a chopped photon source and laser triangulation techniques. Our results are presented and discussed.

Keywords: MEMS, microcantilever, finite element analysis, FEA

1. INTRODUCTION

The desire to shrink the size of mechanical components, optical devices, and sensors to sizes obtained by the microelectronics industry has driven a significant amount of research in the field of micro-electro-mechanical systems (MEMS).[1] Micromechanical devices are currently being considered for a wide variety of applications including uncooled infrared detectors, micro-actuators, chemical detectors, and completed mechanical systems. Currently the dominant manufacturing method for micro-devices is the microlithography approach used by the microelectronics industry' This approach works well for producing a large quantity of devices, however the ability to produce prototype devices is not as developed as the ability to mass-produce devices. The ability to simulate the response of micro-devices using finite element analysis (FEA) gives researchers insight into the behavior of devices before prototypes are developed or production runs occur as well as allowing the designer to optimize the desired response.

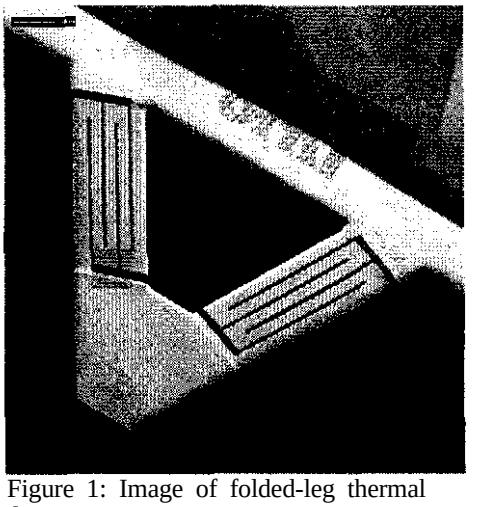

Figure 1: Image of folded-leg thermal detector or pentalever.

Photon detectors[3,4] represent a class of MEMS devices which have been studied with great interest."' Several different types of photon detectors are available including CCDs, microbolometers, thermopiles and pyroelectrics.[5,6] Solid state infrared detectors must be operated at reduced temperatures from the ambient in order to reduce thermal noise.' The infrared thermal detectors discussed here convert the incident radiation into heat which produces a change in the position of the micro-cantilever through bimetallic bending or other effects.[14,8] The goal of this research is to study the effects of several design variables on the bending of microcantilever structures.

'Correspondence: Email: evansbmiii@ornl.gov; Telephone: 423-574-9418; 423-574-407

For this experiment, a "folded-leg" thermal detector was fabricated using focused ion beam milling,' The goal in the design of this device was to create a compact, sensitive, thermal detector, A large collecting area was defined at the end of a folded leg structure to maximize the energy absorbed. The purpose of folding the legs five times was to create a compact device that behaved thermally and mechanically as a larger device. The device with the legs folded five times as shown in Figure 1 is referred to as a pentalever. The collecting area *is* also the area used for optically measuring the displacement.

2. FINITE ELEMENT MODELING

2.1 Finite Element Analysis

The concept of structural finite element analysis involves obtaining an approximate solution for the displacement values of a continuum by dividing that continuum into a number of 'finite elements' and solving the function representing the displacement of those nodal points. Often the energy required to displace the nodes, or strain energy is used to solve the equations. These elements are connected at a specific number of nodal points on their boundary. Functions are chosen to represent the displacement within the finite element based on the nodal displacements. The displacement functions can be used to determine the state of strain within the finite element as a function of the nodal displacements. The knowledge of these strains combined with any existing internal strains and the elastic properties can be used to determine the state of stress within the elements. Existing internal strains would be the result of thermal expansion or other similar phenomena. A system of forces is applied at the nodal points which is equal to any distributed loads or applied boundary stresses such that the system is in equilibrium. The element displacement in terms of the applied and internal forces is given by the following equation:

$$\{F\}_a = [k]_a \{\delta\}_a + \{F\}_{a,p} + \{F\}_{a,\varepsilon o} \tag{1}$$

where $\{F\}_a$ is the matrix representing the force vectors at all of the nodes of an element 'a', $\{F\}_{a,p}$ is the force matrix resulting from applied nodal forces or distributed loads, $\{F\}_{a,\varepsilon o}$ represents forces on the nodes resulting from internal strains, The matrix, [k]. , is the element stiffness matrix, and $\{\delta\}_a$ represents the displacements.[9]

The finite element modeling package Pro/Mechanica was utilized to develop the model for our devices. Pro/Mechanica was chosen for it's high degree of automation in performing optimization studies, and because it uses "geometric" elements. Geometric elements are also referred to as polynomial or 'p' type elements. Although this structure did not take advantage of the p-element's ability to exactly map curved surfaces, we did take advantage of the adaptive meshing and convergence checking ability of the p-element. The ability of the p-element to perform automated geometry optimization was utilized, whereby it would be more time consuming to mesh the geometry during each iteration of optimization.

Designers using finite element analysis are often concerned with descritization errors, or errors associated by modeling a continuous body by a series of fmite elements. Conventional (h-method) finite element codes rely on dividing the structure into a fixed number of elements and solving the matrices associated with those elements and their boundary conditions. Upon solving the matrices associated with the model, the finite element mesh associated with that model is refined by subdividing the elements. Results of each analysis are compared to the previous analysis until the results agree to within a certain percentage. More recently, p-method finite element codes have been introduced which make use of high-ordered polynomial elements. P-element convergence is achieved by increasing the polynomial order of the individual elements. In order to save computational resources the algorithm used by Pro/Mechanica checks the individual elements for convergence and only increases the polynomial order of the elements that have not converged. This type of analysis allows convergence to be checked and accuracy ensured without the need to completely recreate the element mesh. The p-method of finite element analysis was developed in the early 1980's with significant contributions in the literature by 1. Babuska, B. Szabo, and A. Peano, and others."

The displacement and rotation field variables are given in terms of a polynomial series:

$$u = \sum_{i=1}^{n} \begin{bmatrix} u_x^{(i)} \\ u_y^{(i)} \\ u_z^{(i)} \end{bmatrix} I^{(i)} \qquad \beta = \sum_{i=1}^{n} \begin{bmatrix} \beta_x^{(i)} \\ \beta_y^{(i)} \\ \beta_z^{(i)} \end{bmatrix} I^{(i)} \tag{2}$$

where u is the displacement vector and β is the rotation vector. The functions, $\bar{t}$, are the hierarchical polynomial basis functions given by Babuska, Szabo, and Katz.[11,12]

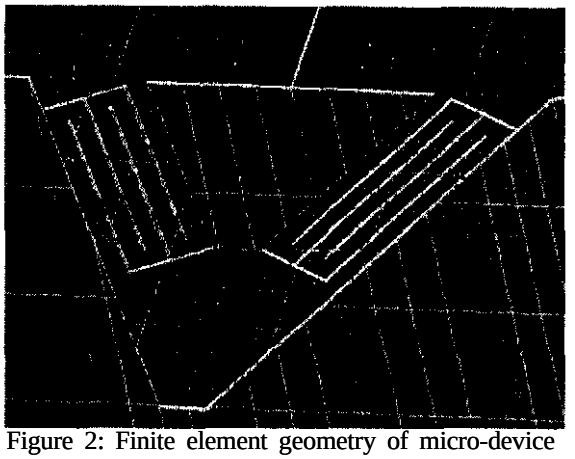

Figure 2: Finite element geometry of micro-device structure.

2.2. FEA Procedure

The FEA model of the micro-device was developed in Pro/Mechanica consisting of 804 two-dimensional shell elements and 1,120 three-dimensional solid elements. The 804 two-dimensional shell elements were used to represent a thin layer of gold on the top of the triangular-shaped cantilever, and the solid elements were used to represent the silicon material in the triangular shaped cantilever and heat sink. The gold layer had a nominal thickness of 50 nanometers, and the cantilever itself had a thickness of 1 micrometer. The base of the triangular shaped cantilever was 200 micrometers and the height was 160 micrometers. The microstructure consists of a large absorbing area near the tip. The legs of the cantilever are folded five times before they attach to the heat sink in order to increase the thermal resistance of the system.

A steady-state analysis was performed on the model using conditions similar to those seen during laboratory experiments with a similar structure. A heat load was applied to the surface of the cantilever equivalent to 0.1μW. The starting temperature of the structure was set to be 0' Centigrade in order to reduce any errors due to round-off or division by very small numbers. Setting the starting temperature at O'C also allows the results to represent the change in temperature. The heat loads were used in a thermal analysis to calculate the deflections caused by the incident, radiant energy. The temperature changes were transferred to the structural analysis and used to calculate the thermal deflection.

A modal analysis was performed to calculate the first four fundamental frequencies of the micro-device, Results of this analysis are used to gain insight into the potential response of the device. Convergence of 10 percent was achieved on all results.

An optimization study was performed to determine the effects of the bimaterial coating thickness on the maximum temperature change and the maximum deflection, In the optimization study, the thickness of the gold coating was varied from 50nm to 50Onm. The analysis was performed to determine the effect of thickness on the maximum temperature change in the cantilever surface and the effect of coating thickness on the maximum temperature obtained by the cantilever. The

Bimaterial microcantilevers are constructed from materials exhibiting dissimilar thermal expansion properties. For example, microcantilevers made from silicon nitride (or silicon) coated with a thin film of gold or platinum will exhibit the bimaterial effect. The bimaterial effect causes the microcantilever to bend in response to temperature variations. The extent of bending is directly proportional to the radiation intensity. Previous work has shown that microcantilever bending can be detected with extremely high sensitivity.[8,14-20] For example, metal-coated microcantilevers that are commonly employed in atomic force microscopy (AFM) allow sub-Angstrom ($< 10^{-10}$ m) sensitivity to be routinely obtained. Recent studies have reported[17-20] the use of microcantilever bending for calorimetric detection of chemical reactions with energies as low as a few pJ. It was demonstrated*' that a similar microcantilever thermal detector had an observed sensitivity of 100 pW corresponding to an energy of 150 fJ and use of the sensor as a femtojoule calorimeter was proposed. An estimate of the minimum detectable power level was on the order of IO pW, corresponding to a detectable energy of 10 fJ and a temperature sensitivity 10^{-5} K. However, using an optimally designed microcantilever, the sensitivity may be improved even further.

The bending of a rectangular bimaterial microcantilever is proportional to the absorbed energy. The maximum deflection, z_{max}, due to differential stress is given by.'",

$$z_{max} = \frac{5}{4}\frac{(t_1+t_2)l^3}{(\kappa_1 t_1+\kappa_2 t_2)wt_2^{\,2}} \times \frac{(\alpha_1-\alpha_2)}{4+6\frac{t_1}{t_2}+6\frac{t_1^{\,2}}{t_2^{\,2}}+\frac{E_1}{E_2}\frac{t_1^{\,3}}{t_2^{\,3}}+\frac{E_2}{E_1}\frac{t_2}{t_1}} \times \eta\left(\frac{dQ}{dt}\right) \tag{3}$$

where l and w are, the length and width of the microcantilever, respectively, t_1 and t_2 are the thickness of the two layers, κ_1, κ_2, a,, α_2, E_1, E_2 are the thermal conductivities; thermal expansion coefficients, and modulus of elasticity of the two layers, and $\eta dQ/dt$ is the fraction of the IR radiation power absorbed. In order to increase the IR detection sensitivity of a microcantilever, z_{max} should be maximized. Note that z_{max} and is strongly dependent on the geometry and thermal properties of the two layers.

3. EXPERIMENTAL

We investigated the response of our devices using the experimental setup shown in Figure 3. To detect movement of the cantilever, a diode laser (delivering 1 mW at 670nm) was focused on the tip of the microcantilever using a 20-power microscope objective. In order to minimize heating of the tip by the probe laser, optical power was reduced by placing a neutral density filter with an optical density of 1.0 between the probe laser and the objective. A quad-element (A,B,C,D) photodiode detector was used to collect the reflected probe beam. The current output ($i_{A,B,C,D}$) of the photodiode depends linearly on the bending of the microcantilever. A high, narrow bandpass optical filter was placed in front of the photodiode allowing the laser beam to be detected while preventing other wavelengths from reaching the photodiode. The amplified differential current signal from the quad cell photodiode, $i_{A,B,C,D}$ [$= (i_A+i_B) - (i_C+i_D) / (i_A+i_B + i_C+i_D)$], was monitored and recorded using a digital oscilloscope (TDS 780,

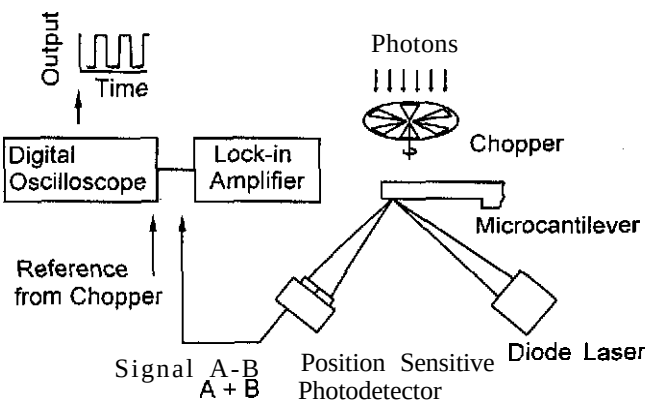

4. RESULTS

4.1. Modeling Results

Modal analysis was performed to determine the first four fundamental frequencies of the device. The results of the modal analysis are shown in Table 1. The mode shape for the fundamental frequency is shown in Figure 4. The analysis of the mode shapes gives insight into the potential dynamic response of the device, as well as the potential motion of the device during excitation.

Table 1: Micro-device natural frequencies.

Mode	Frequency (kHz)
1	12.72
2	41.23
3	47.41
4	84.88

The thermal response of the cantilever to the 1 μW heat load is shown by the temperature distribution in Figure 5. The energy flow from the pad area at the tip through the folded leg geometry is apparent. The temperature change along the path goes from greater than 0.2°C to less than 0.02°C as the thermal energy flows from the pad area to the heat sink. The maximum temperature change in the model when subjected to the 1μW heat load was 0.23°C. Figure 6 shows the thermal bending of the folded leg cantilever. The maximum displacement due to bimetallic bending was 1.86 nm.

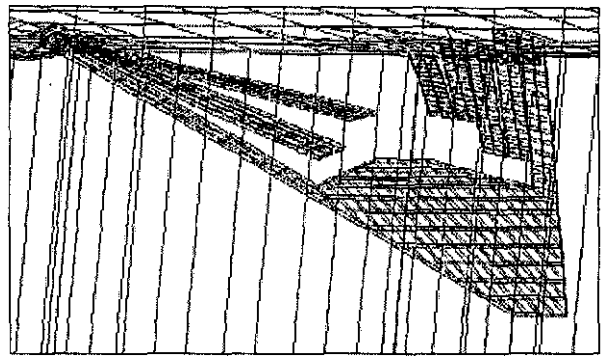

Figure 4: Mode shape of the fundamental frequency.

Optimization studies were performed to predict the tip displacement of the cantilever as a function of energy and to determine the effects of increasing the coating thickness on the displacement of the cantilever. Our results show that the effect of energy on the displacement of the cantilever tip were linear.

Increasing the coating thickness resulted in a decrease in the maximum temperature change achieved in the cantilever. Due to an increase in the bimetallic effect with increased coating thickness, the bending increased to a maximum and then dropped off. The decrease in bending at the greatest coating thickness was due to the overall decrease in thermal resistance. The results of the optimization study are shown in Figure 8, which plots maximum deflection and maximum temperature as a function of coating thickness.

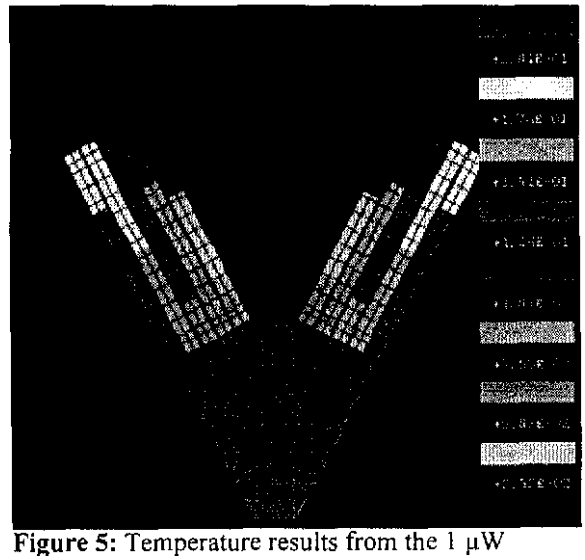

Figure 5: Temperature results from the 1 μW energy load. ΔT in degrees Centigrade.

A steady-state thermal analysis was performed on the cantilever model with the simulated coating applied to alternating legs and both sides of the sensing pad area. For the 1μW heat load the alternating coating geometry experienced a maximum displacement 7.91 nm as opposed to 1.86 nm for the original geometry. These results agree well with preliminary experimental results that show a factor of three improvement in response by alternating the coating. Due to the larger gold-coated area on the alternating coating geometry, the maximum temperature change was 0.226°C as opposed to 0.265°C for the original geometry

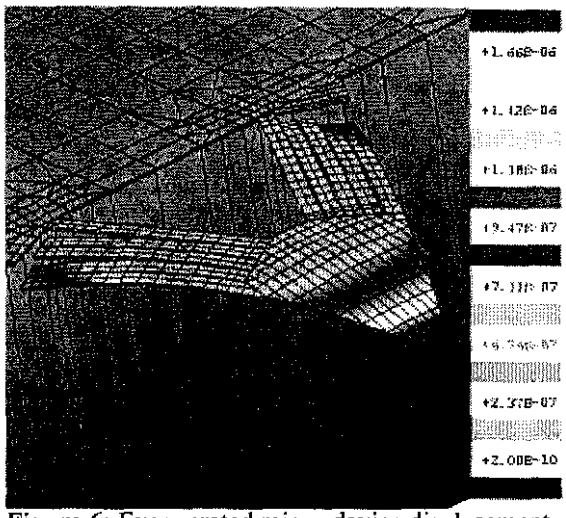

Figure 6: Exaggerated micro-device displacement due to bimetallic bending in mm. Coating only simulated on the top surface.

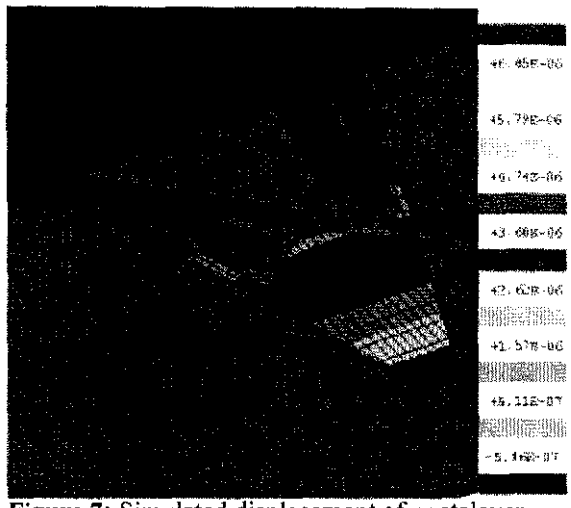

Figure 7: Simulated displacement of pentalever with alternating bimaterial coating on the top and bottom of legs.

Another interesting effect of alternating the coating on the folded leg geometry and coating both sides of the collecting area was that more of a pure rotation of the collector area occurred. The rotation of elements in the center of the collector area was 0.0041" compared to 0.0013" for the device coated entirely on the front surface. The difference in the amount of warping of the collector surface is seen by comparing Figures 6 and 7.

4.2. Thermal Detector Measurements

In order to optimize the thermal detectors used in our micro-

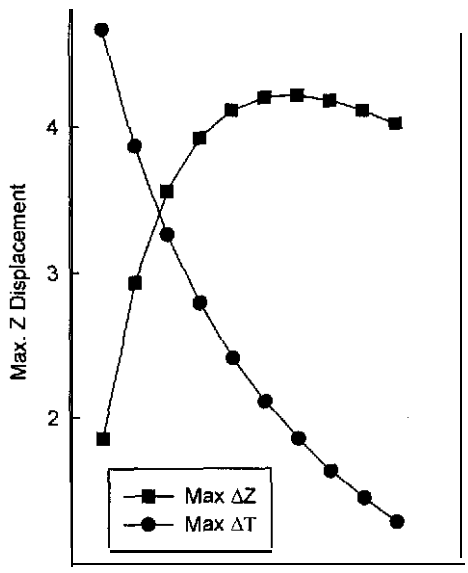

function of the absorbed power, P_{th}, and it can be seen that the maximum bending increases linearly with increasing power. The reflectivity of the gold film is >0.99, and the reflectivity was taken into account when determining the absorbed power. From the slope of the line in Figure 10, we obtained a deflection sensitivity of approximately 0.053 nm/nW. Using a Stanford Research Systems SR 540 chopper to modulate the IR radiation at a frequency of 30 Hz, we calculated a noise equivalent power (NEP) of 520 $pW/Hz^{1/2}$.

The micro-cantilever thermal detector was found to exhibit two distinct thermal response times due to the incoming IR radiation; a time $\tau_{th,1}$

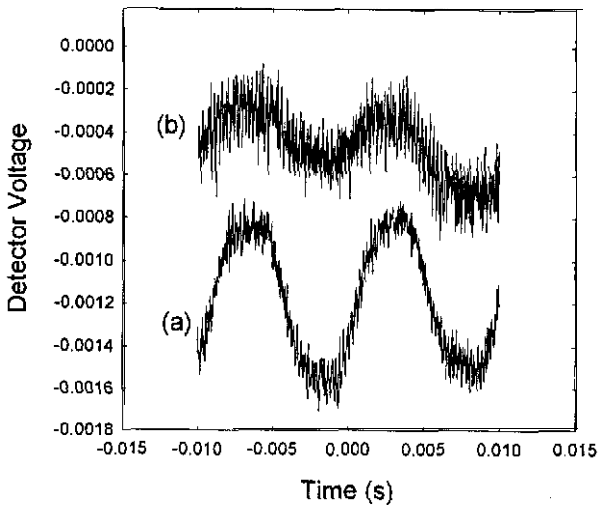

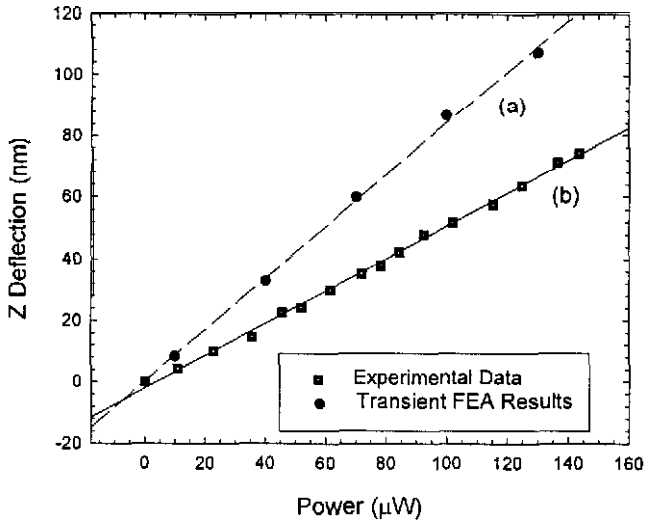

greatest temperature was achieved in the “collector” area at the end of the device, and the temperature can be seen to decrease along the legs of the device indicating heat transfer through the legs of the device itself. Figure 6 illustrates the deformed

REFERENCES

1. M. Madou, *Fundamentals of Microfabrication,* CRC Press, New York, (1997).
2. A. Rogalski, "New Trends in Infrared Detector Technology," Infrared Physics and Technology, 35, 1 (1994).
3. *I.* L. Miller, *Principles of Infrared* Technology (Van Nostram Reinhold, New York, 1994).
4. E. L. Dereniak and G. D. Boreman, *Infrared Detectors and Systems* (Wiley and Sons, New York, 1996).
5. R. A. Wood and N. A. Foss, "Micromechanical Bolometer Arrays Achieve Low-Cost Imaging," Laser Focus World, June, 101 (1993).
6. R. A. Wood, "Uncooled Thermal Imaging with Monolithic Silicon Focal Planes," Infrared Technology XXI, SPIE,
7. S. Rajic, P.G. Datskos, I. Datskou, and T. A. Marlar, "Ultra-responsive thermal sensors for the detection of explosives using Calorimetric Spectroskopy (CalSpec), preprint SPIE Aerosense 1999.
8. P. G. Datskos, P. I. Ode", E. A. Wachter, T. Thundat, and R. J. Warmack, "Remote Infrared Detection Using Piezoresistive Microcantilevers," *Appl. Phys. Lett. 69, 2986 (1996).*
9. O.C. Zienkiewicz, *The Finite Element Method in Structural and Continuum Mechanics,* McGraw-Hill, London, 1967
10. Parametric Technology Corporation, http://www.sj.ptc.com/cs/tech_lib/…nual/AS_2.0_theoretical_manual.htm.
11. Babuska, 1, Szabo, B.A., and Katz, I.N., "The p-Version of the Finite Element Method" *SIAM J. of Num. Anal,* 18,